Drift kinetic effects on plasma response to resonant magnetic perturbation for EU DEMO design

Lina Zhou[1,a], Yueqiang Liu[2,a], Hanqing Hu[1], Mattia Siccinio[3,4], Maviglia Francesco[5], Hartmut Zohm[3], Leonardo Pigatto[6], Yong Wang[7], Li Li[8], Guangzhou Hao[9] and Xu Yang[10]

[1] College of Science, Dalian Maritime University, Dalian 116026, China
[2] General Atomics, PO Box 85608, San Diego, CA 92186-5608, United States of America
[3] EUROfusion Programme, Management Unit, Boltzmannstr 2, D-85748 Garching, Germany
[4] Max-Planck-Institut für Plasmaphysik, Boltzmannstr. 2, 85748 Garching bei München, Germany
[5] EURATOM-ENEA-CREATE, University of Naples Federico II, Napoli 80125, Italy
[6] Consorzio RFX, Corso Stati Uniti, 4 35127 Padova, Italy
[7] Institute of Plasma Physics, HFIPS, Chinese Academy of Sciences, Hefei 230031, Anhui, China
[8] College of Science, Donghua University, Shanghai 201620, China
[9] Southwestern Institute of Physics, PO Box 432, Chengdu 610041, China
[10] Chongqing Key Laboratory of Intelligent Perception and BlockChain Technology, Chongqing Technology and Business University, Chongqing 400067, China

a) Authors to whom any correspondence should be addressed.
E-mail: zhoulina@dlmu.edu.cn, liuy@fusion.gat.com

Abstract

A systematic investigation on the plasma response to the externally applied resonant magnetic perturbation (RMP) field, for the purpose of controlling edge localized modes (ELMs), is carried out for an EU DEMO reference plasma. Particular emphasis is on the role of kinetic effects associated with both thermal particles and fusion-born alphas. The single fluid, resistive model predicts a large peak amplification of the n=1 (n is the toroidal mode number) plasma response for the target equilibrium, which is found to be close to the Troyon no-wall limit. More advanced response model, including kinetic resonances between the RMP perturbation and drift motions of thermal and energetic particles, on the other hand finds strong suppression of the n=1 field amplification. A major role is played by the precessional drift resonance of fusion-born alphas. A strong parallel sound wave damping (SWD) model is found to well reproduce the full kinetic response results for the DEMO plasma, in terms of both the resonant field response

amplitude and the plasma displacement. Finally, both fluid and kinetic models produce similar response for the n=2 and 3 RMP fields for the considered DEMO plasma, whilst kinetic effects again become important for the n=4 RMP due to proximity of the reference plasma to the no-wall limit for the n=4 ideal kink instability.

Keywords: drift kinetic effects, plasma response, EU DEMO

(Some figures may appear in colour only in the online journal)

1. Introduction

It is well known that large scale, low frequency edge localized modes (ELMs), in particular the so-called type-I ELMs, can pose an intolerable material damage in future large fusion devices such as ITER [1] as well as EU DEMO [2]. Among several techniques for ELM control, the resonant magnetic perturbation (RMP), generated by magnetic coils external to the plasma, has been demonstrated to be successful for either suppressing or mitigating type-I ELMs in various tokamak devices, including DIII-D [3, 4], JET [5], NSTX [6], MAST [7, 8], ASDEX Upgrade [9], KSTAR [10], EAST [11], HL-2A [12].

Significant efforts have also been devoted to model various aspects of ELM control with RMP fields [13-39]. It has now been well established that the plasma response to the applied 3D vacuum RMP field plays a crucial role in modifying the ELM behavior [40] as well as the associated plasma transport processes [41, 42]. It is therefore critical to accurately compute the plasma response in order to provide reliable prediction for ELM control in future tokamak devices. In particular, kinetic physics may become

import when the plasma performance is pushed to high levels when designing a future device.

As has previously been shown, the fluid plasma response model, based on ideal magnetohydrodynamic (MHD) theory, predicts a strong amplification of the plasma response field near the Troyon no-wall limit $\beta_{\mathrm{N}}^{\mathrm{NW}}$, being inconsistent with the roughly linear increase of the response with the normalized pressure β_{N} across $\beta_{\mathrm{N}}^{\mathrm{NW}}$ as observed in experiments [4, 6]. Here, $\beta_{\mathrm{N}} = \beta(\%)a(\mathrm{m})B_0(\mathrm{T})/I_P(\mathrm{MA})$, with $\beta = 2\mu_0\langle p\rangle/B_0^2$ being the ratio of the volume averaged plasma pressure $\langle p\rangle$ to the magnetic pressure. B_0 is the magnetic strength at the plasma center, I_p the plasma current, a the plasma minor radius, and μ_0 the vacuum magnetic permeability. This discrepancy between modeling and experiments was resolved by self-consistently including the drift kinetic effects associated with the plasma particle species in the MHD modeling [43], which led to quantitative agreement not only for the measured field amplitude and toroidal phase but also for the measured internal 3D displacement of the plasma [28, 32]. Recently, the MHD-kinetic hybrid model also predicts higher resonant field amplification (RFA) than the fluid model due to a stable resistive wall mode (RWM) response in MAST-U [44]. These results indicate that hybrid MHD-kinetic modeling is essential for determining the plasma response in high β tokamak discharges operating near the Troyon no-wall limit.

In this work, hybrid MHD-kinetic modeling is applied to predict the plasma response to the applied low-n (n is the toroidal mode number) RMP field for an EU DEMO design. Although up to the n=4 response has been modeled in the present study, our focus is on the n=1 response, in view of proximity of β_{N} to $\beta_{\mathrm{N}}^{\mathrm{NW}}$ for the designed target equilibrium. As for the particle kinetic effects, we consider contributions from both thermal and energetic particles, in particular the fusion-born α-particles for the latter, produced by deuterium–tritium reactions in EU DEMO. For

comparison, we also report results obtained by an extended fluid model, where a strong parallel sound wave damping (SWD) model effectively represents the Landau damping physics (due to thermal ions). As a key result, we find that both the direct drift kinetic effect and the strong SWD significantly modify the plasma response to the n=1 RMP field in EU DEMO, in terms of both the response field and the internal plasma displacement. On the other hand, kinetic effects play a minor role in the n=2-4 RMP response for the reference plasma considered.

Section 2 briefly describes the plasma response models implemented into the MARS-F/K codes, which we utilize in this study. Section 3 reports the reference plasma equilibrium adopted for EU DEMO, and analyzes modeling results for the fluid versus kinetic response. Section 4 summarizes the results.

2. Computational models

The fluid and kinetic plasma response to the RMP field is computed with the MARS-F [45] and MARS-K codes [15, 43], respectively. Both codes solve perturbed single fluid (MHD) equations in full toroidal geometry. In addition, the MARS-K formulation adopts a closure equation (for the perturbed plasma pressure) coming from the solution of the drift-kinetic equation for plasma particle species (both thermal and energetic particles). For better understanding of the numerical results presented later on, we provide below a brief description of the model that allows a continuous transition from the single fluid model implemented in MARS-F, to the non-perturbative MHD-kinetic hybrid model implemented in MARS-K. Detailed model formulations can be found in Refs. [15,43,45]. The MHD-kinetic hybrid equations in the plasma region are written in the Eulerian frame

$$i\left(\Omega_{\text{MP}}+n\Omega\right)\boldsymbol{\xi}=\boldsymbol{v}+\left(\boldsymbol{\xi}\cdot\nabla\Omega\right)R^2\nabla\phi, \tag{1}$$

$$\begin{aligned} i\rho\left(\Omega_{\text{MP}}+n\Omega\right)\boldsymbol{v}=&-\nabla\cdot\boldsymbol{p}+\boldsymbol{j}\times\boldsymbol{B}+\boldsymbol{J}\times\boldsymbol{b}\\ &-\rho\left[2\Omega\hat{\boldsymbol{Z}}\times\boldsymbol{v}+\left(\boldsymbol{v}\cdot\nabla\Omega\right)R^2\nabla\phi\right]-\nabla\boldsymbol{\Pi}, \end{aligned} \tag{2}$$

$$i\left(\Omega_{\text{MP}}+n\Omega\right)\boldsymbol{b}=\nabla\times\left(\boldsymbol{v}\times\boldsymbol{B}\right)+\left(\boldsymbol{b}\cdot\nabla\Omega\right)R^2\nabla\phi-\nabla\times\left(\eta\boldsymbol{j}\right), \tag{3}$$

$$i\left(\Omega_{\mathrm{MP}}+n\Omega\right)p=-\boldsymbol{v}\cdot\nabla P-\left(1-\alpha_{\mathrm{k}}\right)\Gamma P\nabla\cdot\boldsymbol{v}, \tag{4}$$

$$j=\nabla\times\boldsymbol{b}, \tag{5}$$

$$\boldsymbol{p}=p\boldsymbol{I}+\alpha_{\mathrm{k}}p_{\parallel}\hat{\boldsymbol{b}}\hat{\boldsymbol{b}}+\alpha_{\mathrm{k}}p_{\perp}(\boldsymbol{I}-\hat{\boldsymbol{b}}\hat{\boldsymbol{b}}), \tag{6}$$

$$p_{\parallel}=\sum_{j}M_{j}v_{\parallel}^{2}f_{L}^{1}dV,\ p_{\perp}=\sum_{j}\frac{1}{2}M_{j}v_{\perp}^{2}f_{L}^{1}dV \tag{7}$$

where ρ, $\boldsymbol{B}$ and $\boldsymbol{J}$ are the equilibrium plasma density, magnetic field and current density, respectively. P is the total equilibrium pressure (including that of thermal and energetic particle contributions). The perturbed quantities $\boldsymbol{\xi}$, $\boldsymbol{v}$, $\boldsymbol{b}$, $\boldsymbol{j}$, $\boldsymbol{p}$ represent the plasma displacement, perturbed velocity, magnetic field, current density and pressure, respectively. $\hat{\boldsymbol{Z}}$ and $\hat{\boldsymbol{R}}$ are unit vectors in the vertical and major radius directions, respectively, on the poloidal plane. The rotation frequency of the RMP field is chosen to be $\Omega_{\mathrm{MP}}=0$, i.e., the RMP coils are powered to produce dc-currents in this study. Ω is the angular frequency of the plasma equilibrium toroidal flow along the geometric toroidal angle ϕ of the torus.

The plasma resistivity is denoted by η in Eq. (3), which is inversely proportional to Lundquist number $S=\tau_{\eta}/\tau_{\mathrm{A}}$, where τ_{η} and τ_{A} are resistive diffusion time of the plasma current and toroidal Alfven time, respectively. The Spitzer model is used for estimating the plasma resistivity, yielding the on-axis Lundquist number of $S\sim10^{11}$ for the reference EU DEMO plasma. Γ = 5/3 is the ratio of specific heats. α_{k} is a numerical parameter introduced to allow a continuous transition from the single fluid formulation (at $\alpha_{\mathrm{k}}=0$) to the MHD-kinetic hybrid formulation (at $\alpha_{\mathrm{k}}=1$).

The last term in equation (2), $\nabla\boldsymbol{\Pi}=\rho\kappa_{\parallel}\left|k_{\parallel}v_{\mathrm{th,i}}\right|\boldsymbol{v}_{\parallel}$, represents a viscous term describing the parallel sound wave damping physics, where $k_{\parallel}$ is the parallel wave number and $v_{\mathrm{th,i}}$ the thermal ion velocity. $\kappa_{\parallel}$ is a numerical coefficient specifying the 'strength' of the SWD. Physically, this model describes the Landau damping of the parallel sound waves due to the ion-acoustic resonances [45]. The SWD model can thus be viewed as a kinetic correction to the standard MHD model, specifically along the parallel motion, in the presence of equilibrium flow [46]. At low plasma pressure, this damping term has minor effect on the plasma response [4], whilst the strong SWD better describes the experimental results in higher-β plasmas [27, 47]. In this work, we

shall investigate the sensitivity of the computed plasma response against the choice of $\kappa_{\|}$.

The direct drift-kinetic effects self-consistently enter MHD equations via the perturbed kinetic pressure tensor $\boldsymbol{p}$ in Eq. (2). As shown in Eq. (6), the perturbed pressure tensor $\boldsymbol{p}$ consists of a scalar component p (the so-called adiabatic contribution, representing the fluid pressure perturbation) and the anisotropic tensor components describing the non-adiabatic contributions. The tensor terms consist of components parallel ($p_{\|}$) and perpendicular ($p_{\perp}$) to the equilibrium field lines. The symbol $\boldsymbol{I}$ denotes the unit tensor here, and $\hat{\boldsymbol{b}} = \boldsymbol{B}/|B|$ is the unit vector along the equilibrium magnetic field line (not to be confused with the perturbed magnetic field $\boldsymbol{b}$). The drift-kinetic pressure perturbations are calculated from Eq. (7), where V signifies the velocity space of the particles, and j represents the particle species, including the thermal ions and electrons as well as the fusion-born α-particles in this study. M_j is the corresponding particle mass. $v_{\|}$ and $v_{\perp}$ denote the parallel and perpendicular velocities of the particle guiding center drift motion, respectively. f_L^1 is the non-adiabatic perturbed distribution function as the solution of the drift-kinetic equation for each particle species [43]. A key component in the drift-kinetic solution is the mode-particle resonance operator [43]

$$\lambda_{ml} = \frac{n\left[\omega_{*N} + \left(\hat{\varepsilon}_k - \frac{3}{2}\right)\omega_{*T} + \omega_E\right]}{n\omega_d + \left[\alpha\left(m + nq\right) + l\right]\omega_b - i\nu_{eff}} \tag{8}$$

with ω_{*N} and ω_{*T} denoting the diamagnetic drift frequencies associated with the plasma density and temperature gradients, respectively. ω_E is the $\boldsymbol{E}\times\boldsymbol{B}$ drift frequency due to the equilibrium electrostatic potential. ω_d is the bounce-orbit-averaged toroidal precession drift frequency of particles, including the ω_E drift. ω_b is the particle bounce/transit frequency. $\hat{\varepsilon}_k$ is the particle kinetic energy normalized by temperature. l is the Fourier harmonic index over the particle bounce orbit. $\alpha = 1$ for passing particles, and $\alpha = 0$ for trapped particles. ν_{eff} is the effective particle collision frequency. Note that we assume a Maxwellian equilibrium distribution function for thermal particles, and an isotropic (in particle pitch angle) slowing-down (in particle energy) equilibrium distribution function for α-particles [48].

3. Numerical results

3.1. Reference equilibrium and RMP coil configurations

A reference plasma equilibrium from the EU DEMO design [49], produced by the ASTRA code transport simulation [50], is adopted for this study. The key plasma parameters are: the plasma major radius $R_0 = 8.938$ m and the aspect ratio $A = R_0/a = 3.1$, the on-axis vacuum toroidal field $B_0 = 5.74$ T, the total plasma current $I_p = 18$ MA and the normalized pressure $\beta_N = 2.78$. Figure 1 shows the plasma boundary shape and the modelled shapes for the vacuum vessels (VVs) with a double wall structure, together with the geometry of the ELM control coils. The control coils are centered at the outboard mid-plane of the torus, with the poloidal coverage of $\Delta\theta = 74^o$. This is partly motivated by an coil geometry optimization study for EU DEMO, showing that the resonant field increases with the coil size $\Delta\theta$ for the lower-n (in particular n = 1) RMP field, for the single mid-plane row of coils [33]. In this study, we shall consider three possible radial locations for the coils based on the EU DEMO design: $r_c = 1.9a$ (just inside the outer vacuum vessel), $r_c = 2.6a$ and $r_c = 2.9a$ (both external to the VVs). From the viewpoint of maximizing the applied field (at a fixed coil current), coils located closer to the plasma (e.g., $r_c = 1.9a$) are certainly more desirable. On the other hand, engineering constraints, as well as the potentially hazard environment inside the vacuum vessel, make it preferable to install the coils outside the VVs (e.g. $r_c = 2.6a$ or $r_c = 2.9a$) in DEMO. In this study, unless stated otherwise, we assume the ELM control coil location at $r_c = 1.9a$.

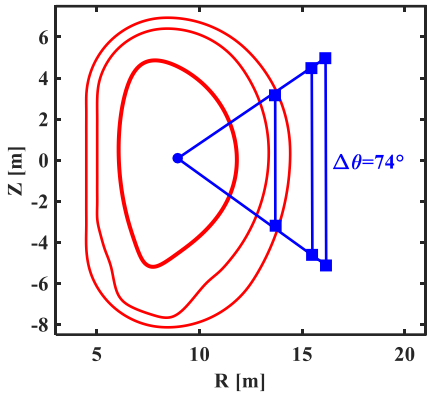

Figure 1. (Color online) The plasma boundary shape for the EU DEMO 18 MA reference equilibrium, plotted together with the smoothed shapes of double vacuum vessels (VV) and the outboard mid-plane ELM control coils (in blue) assuming three radial locations: $r_c \approx 1.9a,\ 2.6a,\ 2.9a$. The coverage of the middle-row coils along the geometric poloidal angle is chosen to be $\Delta\theta = 74^{o}$.

Figure 2 shows radial profiles for key equilibrium quantities that are relevant to our study. The plasma density (Fig. 2(a)) is normalized to unity at the magnetic axis. The equilibrium pressure (Fig. 2(a), shown by the second vertical axis on the right) is normalized by B_0^2/μ_0. An important approximation here is the toroidal rotation profile, which has so far not been properly predicted for DEMO. The rotation profile shown in Fig. 2(b) is thus *ad hoc* chosen, resembling that predicted for ITER [26]. The amplitude of the rotation frequency at the magnetic axis is varied from $0.005\omega_A$ to $0.015\omega_A$ ($\omega_A = B_0/\left[R_0\sqrt{\mu_0\rho_0}\right]$ is the on-axis toroidal Alfven frequency), considering significant uncertainty in predicting the toroidal rotation in EU DEMO.

The equilibrium toroidal current density (solid blue curve in Fig. 2(c), i.e. J_1) from the DEMO design has a large bootstrap current component near the plasma edge, which prduces a strong peeling instability as will be shown later on. To eliminate this peeling-drive, as well as to investigate the role of the edge localized bootstrap current on the plasma response, we also consider a slightly modified current density profile as shown

by the dashed red curve (i.e. J_2) in Fig. 2(c). This modification does not affect the global safety factor profile as shown in Fig. 2(d), but does change the edge q-value. Note that we shall adopt the original equilibrium (i.e. with the J_1-model for the toroidal current density profile) for investigating the fluid and kinetic plasma response. The safety factor in Fig. 2(d) has the on-axis value of $q_0 = 1.07$ and $q_{95} = 4.2$ at the 95% equilibrium poloidal flux surface for the original equilibrium.

The equilibrium density and pressure profiles for the fusion-born alpha particles are simulated by the ASCOT code [51] and are shown in Fig. 2(e) and (f), respectively. Note that the alpha density and pressure profiles are normalized by the corresponding thermal electron density and thermal pressure, respectively. For this EU DEMO design, alpha particles contribute about 60% of the thermal fraction to the equilibrium pressure, with about 3.5% of the density fraction. The equilibrium distribution for alphas is assumed to be isotropic in particle pitch angle and slowing-down in particle energy [48, 52]. For fusion-born alphas, this type of equilibrium distribution can be analytically calculated by solving the Fokker–Plank equation with simplifying assumptions [53].

In what follows, we shall determine the Troyon no-wall limits first based on ideal kink stability computations by MARS-F, for the n=1-4 perturbations. This is followed by a detailed report on the n=1 plasma response computations taking into account various plasma effects: the roles of the equilibrium pressure and toroidal rotation, the fluid versus kinetic plasma response, the role of the parallel sound wave damping in the plasma response for the DEMO plasma under consideration. Next, we investigate the sensitivity of the results against radial location of the assumed RMP coils. Finally, plasma response for the n=2-4 RMP fields will also be reported.

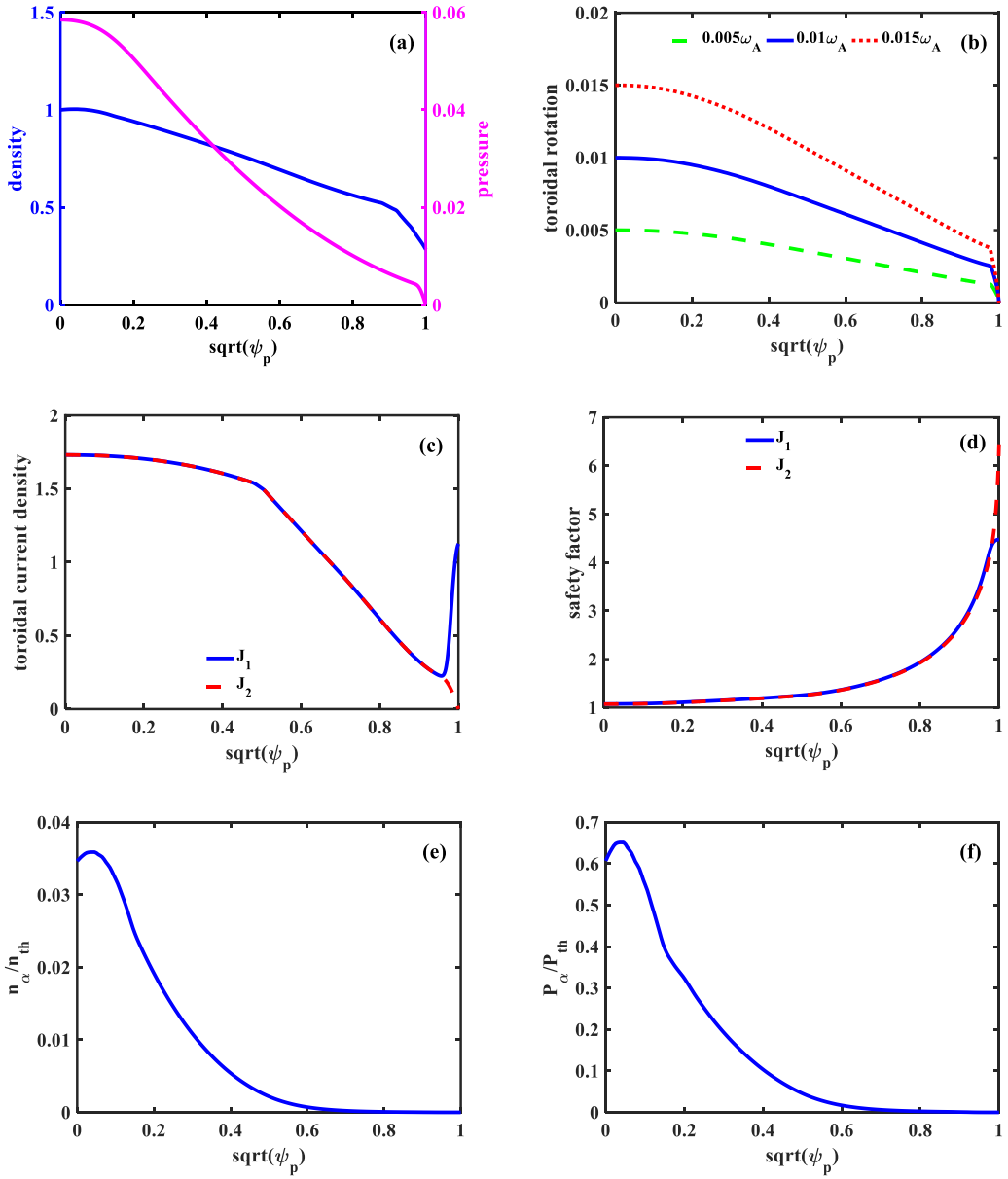

Figure 2. (Color online) Equilibrium radial profiles for (a) the plasma density (normalized to unity at the magnetic axis) and the pressure (normalized by B_0^2/μ_0, shown by the right-hand side vertical axis), (b) the (assumed) plasma toroidal rotation frequencies normalized by the Alfven frequency ω_A, (c) the two choices of the surface averaged toroidal current density normalized by $B_0/(\mu_0 R_0)$ (with μ_0 being the vacuum magnetic permeability), and (d) the safety factor q corresponding to the two current density profiles from (c). Shown are also the equilibrium radial profiles for the (e) density and (f) pressure of fusion-born alpha particles, normalized by the

corresponding thermal electron density and total thermal pressure, respectively. Here, $\sqrt{\psi_p}$ labels the plasma radial coordinate with ψ_p being the normalized equilibrium poloidal magnetic flux.

3.2. No-wall stability limits and plasma response with varying pressure and plasma flow

As mentioned earlier, comparative modeling studies of the DIII-D and NSTX experiments have shown that a full drift kinetic model is essential for reliably predicting the plasma response in high β tokamak plasmas, especially when the plasma pressure approaches (or even exceeds) the no-wall beta limit for the ideal kink mode [28, 32]. For the EU DEMO plasma, we therefore start by computing the n=1-4 ideal kink stability, in order to identify the Troyon no-wall limit β_N^{NW} [54]. The results are reported in Fig. 3, where we scan the overall pressure amplitude (thus β_N) with fixed radial profile, and compute the growth rate of the ideal kink instability without a wall. For the original equilibrium (i.e. the J_1-model), the ideal instability is driven by both the plasma edge bootstrap current (peeling mode) and pressure (kink-ballooning mode), resulting in two branches. The no-wall limit is established by tracing the pressure-driven branch in this case. With the modified equilibrium (with the J_2-model), where the edge current drive is eliminated, only the pressure-driven branch is unstable.

Figure 3 shows that the Troyon no-wall limits are $\beta_N^{NW} = 2.9,\ 3.5,\ 3.7,\ 3.2,$ for n=1-4 ideal external kinks, respectively, based on the modified equilibrium. Slightly lower limits are computed for the original equilibrium, if we ignore the edge current driven peeling instability. We also note that the target β_N value of 2.78 is close to β_N^{NW} =2.9 for the n=1 instability. This has significant implications on the plasma response to the RMP field for the reference plasma, reported in Fig. 4.

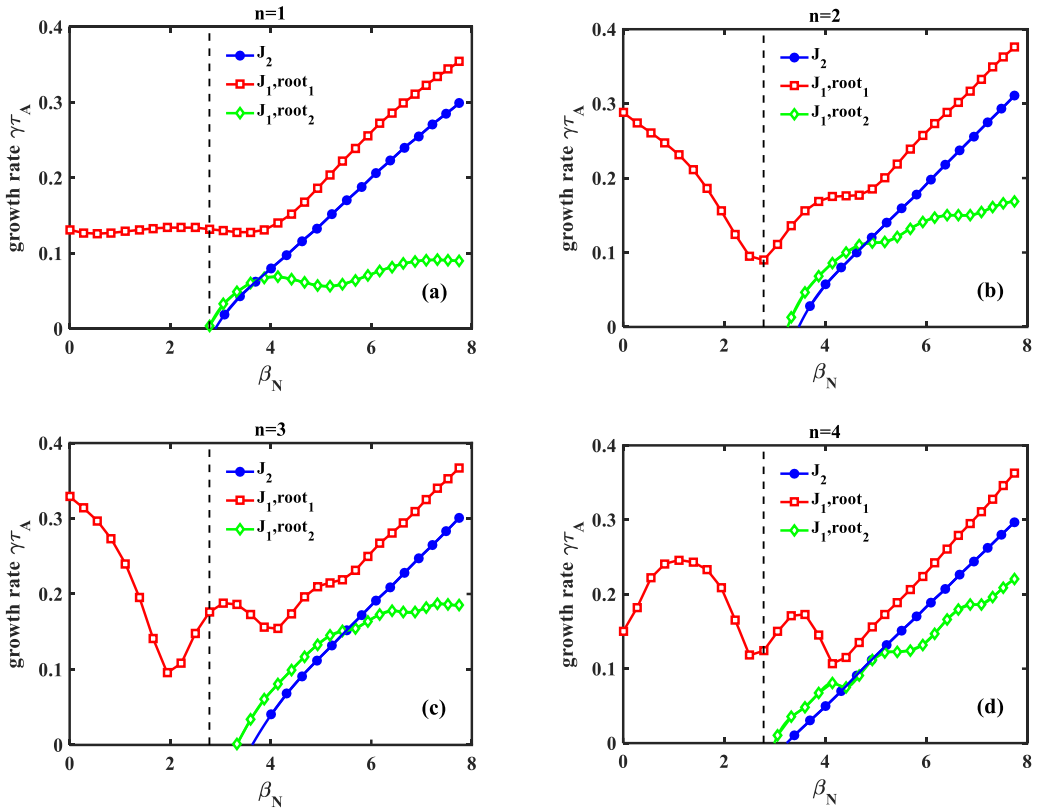

Figure 3. (Color online) The MARS-F computed growth rate of the no-wall ideal instabilities while varying the normalized pressure β_N, for the (a) n=1, (b) n=2, (c) n=3, and (d) n=4 modes. The legends J_1 and J_2 indicate the corresponding toroidal current density profiles shown in Fig. 2(c). Two unstable roots are computed for the equilibrium with the J_1-profile. Vertical dashed lines indicate the DEMO design value of $\beta_N = 2.78$.

Figure 4 plots the MARS-F computed plasma response to the n=1 RMP field - both amplitude and toroidal phase and for the original equilibrium current density profile - while varying the plasma pressure for the three choices of the plasma toroidal rotation shown in Fig. 2(b). The plasma response here is measured by the maximal amplitude of the n=1 radial magnetic field b^1 along the minor radius, for the resonant poloidal Fourier harmonic associated with the rational surface near the plasma edge. This choice is partly motivated by the fact that the resonant field amplification

phenomenon, which we investigate in this work, is better quantified in terms of the overall amplitude of the plasma response. Indeed, as shown here in Fig. 4 as well as in later figures, this choice of metric well recovers the general trend found in previous experimental modeling work [28, 32].

Several interesting observations can be made here. First, at relatively low equilibrium pressure ($\beta_N < 2.5$), a nearly linear increment of the plasma response is computed by the fluid model. The fluid response however drastically increases at the target pressure (indicated by vertical dashed lines) which is close to the n=1 no-wall limit. This behavior is consistent with the previous modeling results with the fluid model for DIII-D [28] and NSTX [28, 32]. However, as pointed out in these previous studies, the significant amplification by the fluid model (towards the no-wall limit) does not agree with experimental observations [5]. The results reported in Fig. 4 thus points to the necessity of including drift kinetic effects in the plasma response computations for this DEMO plasma scenario, which is our subject of study in subsection 3.3.

As for the next interesting observation from Fig. 4(a), we note that the toroidal plasma rotation plays a minor role in determining the plasma response when the plasma pressure is well below the no-wall limit. However, the plasma flow strongly affects the fluid response at the target pressure, by reducing the field amplification effect. This is understood as the flow screening effect on the resonant magnetic field perturbation. Finally, a significant change of the toroidal phase of the plasma response – from about 0^o at low pressure to about 180^o at the target pressure – is predicted by the fluid model (Fig. 4(b)). This large phase variation is not sensitive to the assumed plasma rotation, when the plasma pressure is below the no-wall limit.

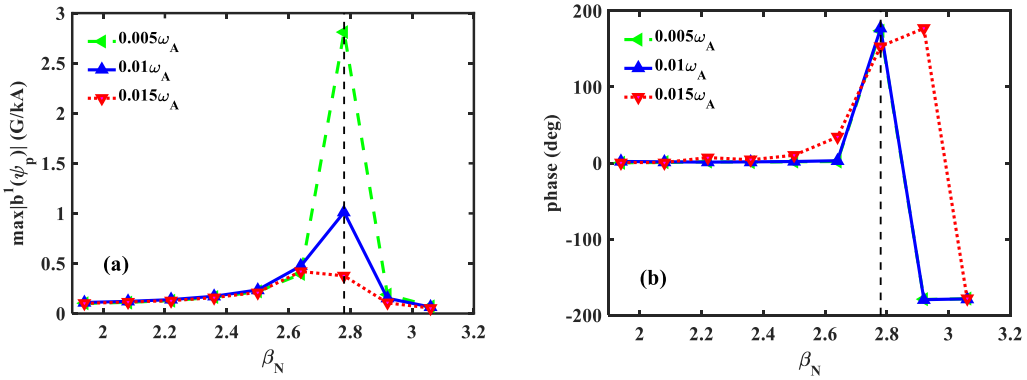

Figure 4. (Color online) The MARS-F computed (a) maximal amplitude (along the minor radius), and (b) the associated toroidal phase, of the n=1 radial magnetic field b^1 for the outermost resonant poloidal Fourier harmonic (m=4) inside the plasma, with the original equilibrium current density (model 'J_1' from Fig. 1(c)), while varying the normalized plasma pressure β_N. The field perturbation results from the plasma response to the applied RMP field with a unit coil current. Compared are results assuming three different (on-axis) plasma toroidal rotation frequencies: $0.005\omega_A$, $0.01\omega_A$ and $0.015\omega_A$ as shown in Fig.2 (b). Vertical dashed lines indicate the DEMO design value of $\beta_N = 2.78$. The RMP coils are located at $r_c = 1.9a$.

Figure 4 only shows the maximal amplitude along the minor radius for the resonant radial field component $b^1(m/n=4/1)$. Figure 5 compares the full poloidal spectrum of the response field among four specific examples with different pressure and rotation values. It is evident that, at fixed β_N, plasma rotation mainly affects the overall amplitude of the spectrum without impacting the spectrum pattern. The plasma response induced field amplification mainly occurs in the spectral domain with positive helicity, i.e. for $m>0$ harmonics, that approximately align with the pitch of the equilibrium field lines. The strongest amplification occurs at the non-resonant portion of the spectrum (m=2) in the plasma core for this EU DEMO plasma, as shown in Fig.

5(a) and (b). This core amplification, on the other hand, is not prominent at lower plasma pressures, such as for the $\beta_N = 2.5$ case shown in Fig. 5(c) and (d).

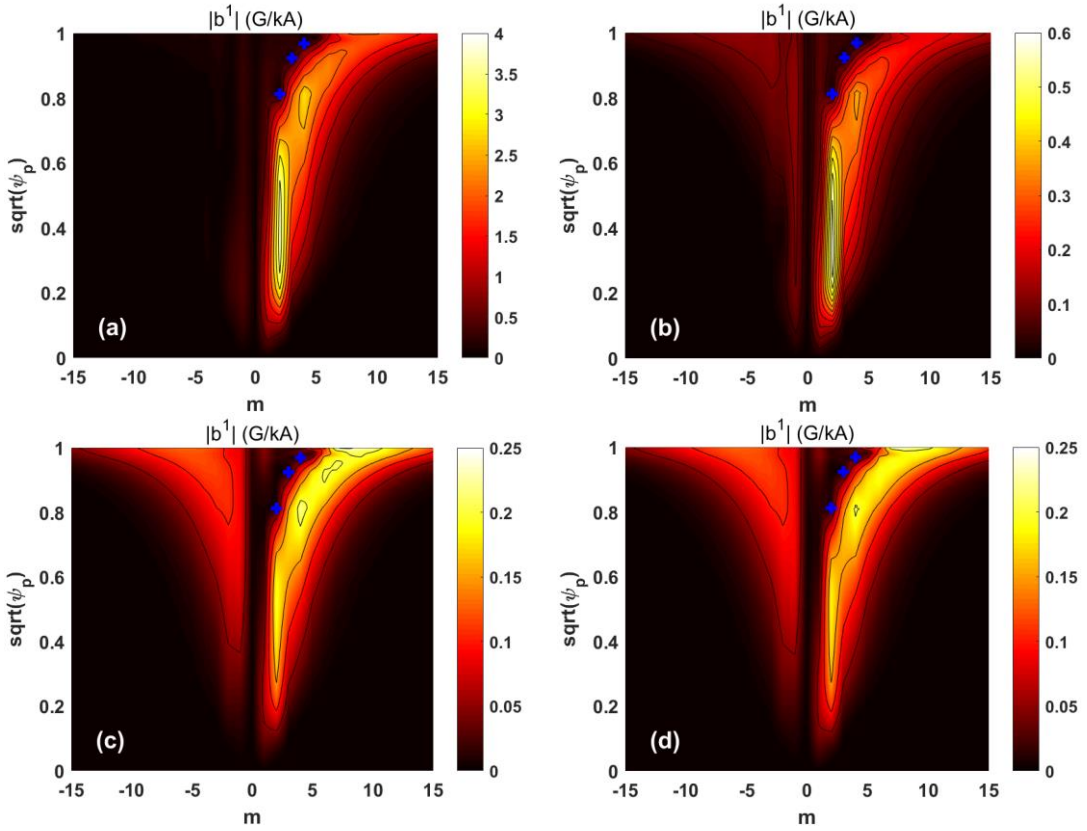

Figure 5. (Color online) Comparison of the poloidal spectra for the whole plasma region, of the *n*=1 perturbed radial magnetic field computed with the fluid model and assuming the (on-axis) plasma toroidal rotation frequency of (a,c) $\Omega = 0.005\omega_A$ and (b,d) $\Omega = 0.015\omega_A$. Symbols '+' indicate the location of the q = m/n rational surfaces. The field perturbation results from the plasma response to the applied RMP field with a unit coil current. Considered are two equilibria, with the normalized pressure of (a,b) $\beta_N = 2.78$ and (c,d) $\beta_N = 2.5$, respectively. The RMP coils are located at $r_c = 1.9a$.

3.3. Fluid versus kinetic plasma response to n=1 RMP

As stated earlier, kinetic effects of thermal particles become important for the plasma response as the plasma pressure approaches β_N^{NW}, which is the case for the n=1 RMP in the EU DEMO plasma scenario considered here. Furthermore, due to substantial contribution of fusion born α-particles to the equilibrium pressure, kinetic effects of these EPs may also be important. Figure 6 compares the computed maximal amplitude and toroidal phase along the minor radius of the m/n=4/1 radial magnetic field b^1, between the fluid and MHD-kinetic hybrid models. Compared are also the kinetic response including kinetic contributions from various particle species. More specifically, we consider three cases of kinetic response, which all include the adiabatic contribution from both thermal particles (TPs) and energetic particles (EPs). The difference is in the non-adiabatic contribution, which is included separately for TPs or EPs, or all together.

As reported earlier, the fluid response ('Fluid') shows a large amplification and a significant phase change near the DEMO design value of $\beta_N = 2.78$. This behavior is absent with the higher-fidelity response models including drift kinetic effects, as shown in Fig. 6. We also mention that this smooth transition of the modeled kinetic response across the no-wall limit is not very sensitive to the uncertainty in the assumed toroidal rotation. Furthermore, the 'EP+TP' case shows similar behavior to the 'EP' case, indicating that the drift kinetic effect from EPs plays a major role in modifying the plasma response in this DEMO plasma. We note that this is different from the modeling results reported for DIII-D [28] and NTSX [32], where kinetic effects from TPs were found to play a dominant role in determining the kinetic response.

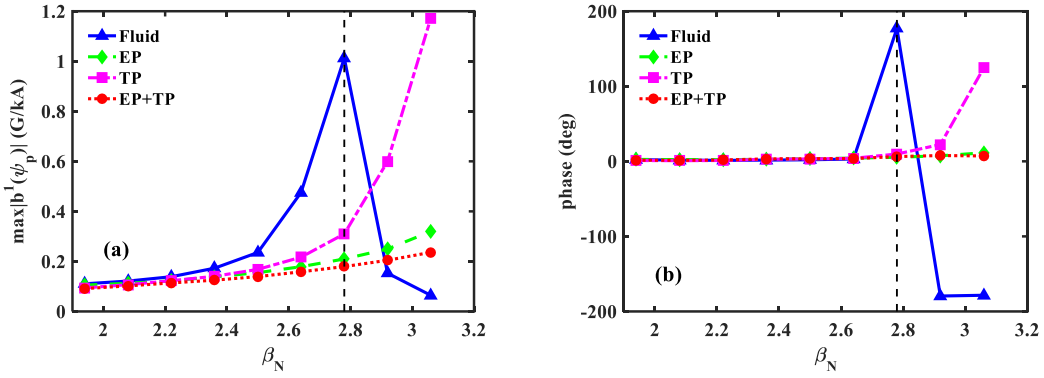

Figure 6. (Color online) The (a) maximal amplitude (along the minor radius), and (b) associated toroidal phase, of the n=1 radial magnetic field perturbation b^1 for the outermost resonant poloidal Fourier harmonic (m=4) inside the plasma, plotted versus the normalized plasma pressure β_N and assuming the (on-axis) toroidal rotation frequency of $\Omega = 0.01\omega_A$. Compared are the response fields obtained assuming the fluid model ('Fluid'), and the MHD-kinetic hybrid model including the non-adiabatic contributions from energetic particles ('EP', i.e. fusion-born alphas) or thermal particles ('TP'), or both ('EP+TP'). Vertical dashed lines indicate the DEMO design value of $\beta_N = 2.78$. The RMP coils are located at $r_c = 1.9a$.

A more comprehensive understanding of the drift kinetic effect on the plasma response is provided by comparing the poloidal spectra as shown in Fig. 7. Here, the fluid response is again compared with kinetic response including various particle contributions, but for the reference plasma at $\beta_N = 2.78$. As indicated by the difference in color scales for four cases, kinetic effects significantly reduce the overall amplitude of the response spectrum, avoiding the singular-like amplification predicted by the fluid model. Furthermore, the similarity of the poloidal spectra between the 'EP' case (Fig. 7(b)) and the 'EP+TP' case (Fig. 7(d)) again reveals that, in our case, energetic particles contribute to the predominant kinetic effect in modifying the fluid plasma response. More specifically, the non-adiabatic contribution from fusion-born alphas is the main

factor for eliminating the strong amplification in the fluid response, especially for the non-resonant portion of the fluid spectrum (m=2) in the plasma core. This is not surprising given the core-localized distribution of fusion-born alphas as shown in Fig. 2(e-f). Thermal particles help to reduce the overall response but do not eliminate the core amplification.

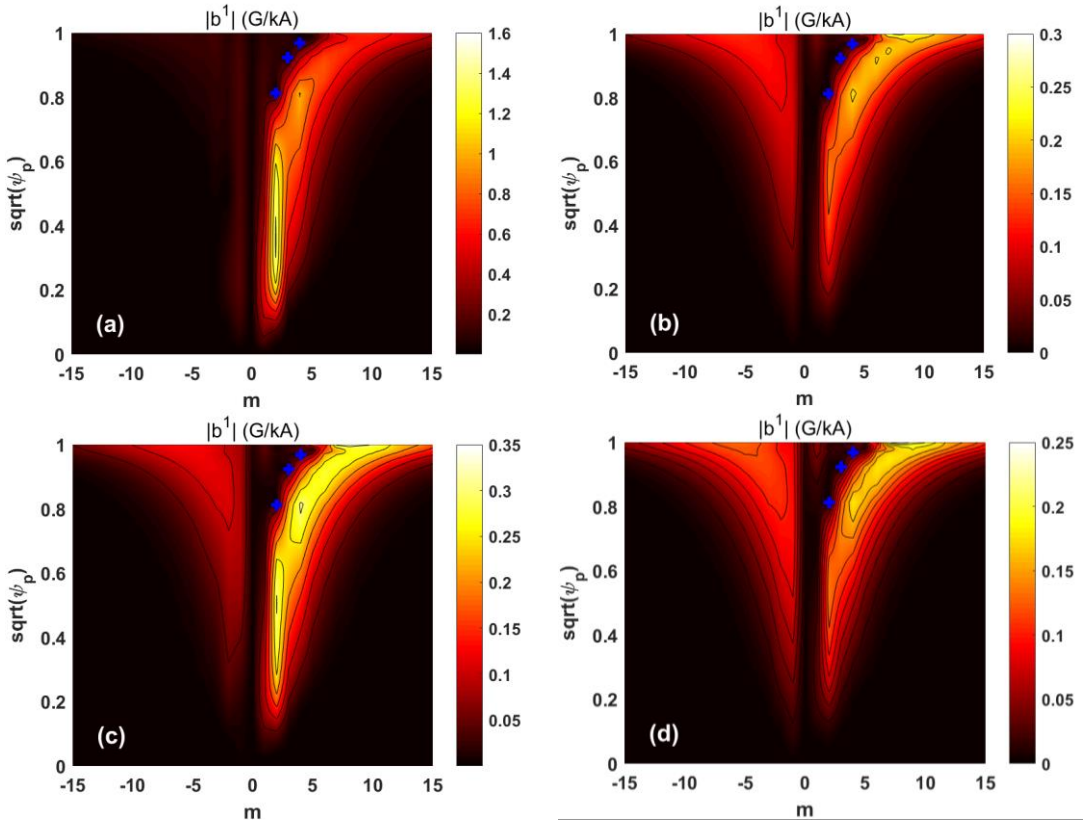

Figure 7. (Color online) Comparison of the poloidal spectra of the n=1 perturbed radial magnetic field assuming (a) the fluid model, and the MHD-kinetic hybrid model including non-adiabatic contributions from (b) fusion-born alphas, (c) thermal particles or (d) both alphas and thermal particles. Symbols '+' indicate the location of the q = m/n rational surfaces. The field perturbation results from the plasma response to the applied RMP field with a unit coil current. Considered is the EU DEMO reference plasma with $\beta_N = 2.78$ and assuming the on-axis toroidal rotation of $\Omega = 0.01\omega_A$. The RMP coils are located at $r_c = 1.9a$.

We have so far been comparing the plasma response in terms of the perturbed radial field. Another important figure of merit, especially for judging the ELM control by RMP, is the plasma displacement [19,40]. Figure 8 compares the computed radial displacement of the plasma, as a result of response to the applied RMP field, between the fluid and kinetic models for the DEMO reference equilibrium and assuming the on-axis rotation of $\Omega = 0.01\omega_A$. Compared with the fluid response shown in Fig. 8(a), the amplitude of the plasma displacement is also strongly suppressed by the kinetic effects. (Note that the same color scale is applied for all four plots in this figure.) More precisely, kinetic effects from thermal particles reduce the fluid displacement by about one order of magnitude. Including non-adiabatic contributions from both thermal and energetic particles, the maximal displacement is reduced by a factor of about 30 as compared with the fluid counterpart. Note also the significant modification of the internal response structure in the plasma core region, by the particle drift kinetic effects. These results highlight the importance of self-consistent MHD-kinetic modeling of the plasma response to the RMP field for the reference DEMO plasmas.

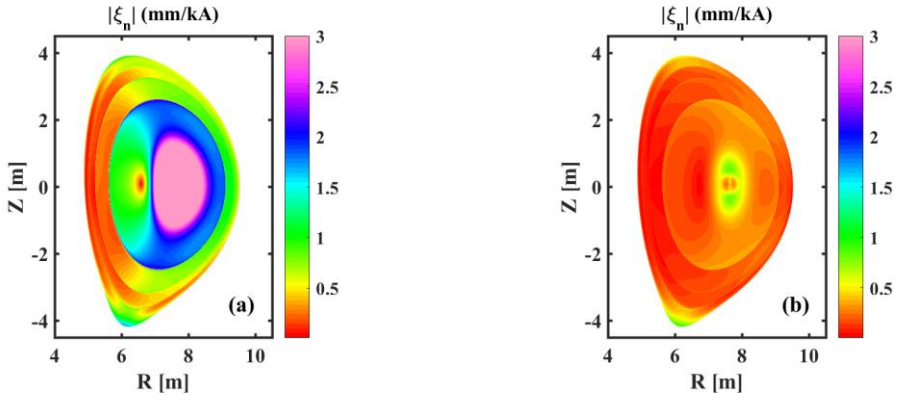

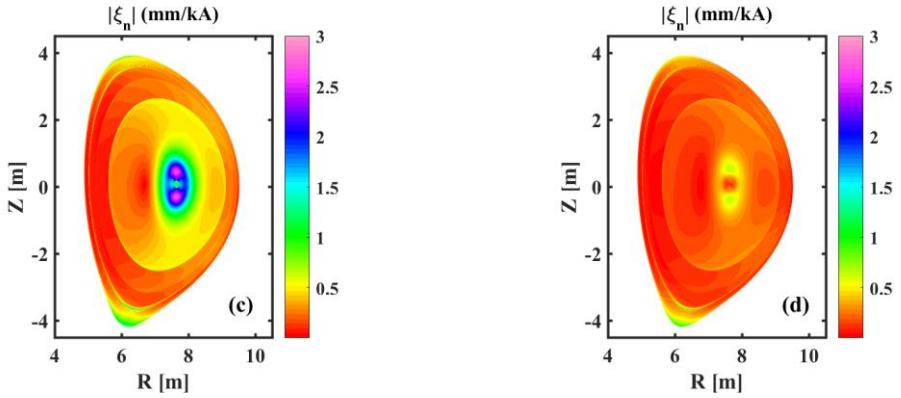

Figure 8. (Color online) Comparison of the amplitude of the normal component of the computed plasma radial displacement, due to the plasma response to the applied *n*=1 RMP field with a unit coil current in DEMO, assuming (a) the fluid model, and the MHD-kinetic hybrid model including non-adiabatic contributions from (b) fusion-born alphas, (c) thermal particles, and (d) both alphas and thermal particles. Considered is the EU DEMO reference plasma with $\beta_N = 2.78$ and assuming the on-axis toroidal rotation of $\Omega = 0.01\omega_A$. The RMP coils are located at $r_c = 1.9a$.

It is also of particular interest to compare the plasma response at the plasma boundary, for both the normal field and normal displacement [15]. These are illustrated in Fig. 9, where the amplitude of these normal components is plotted versus the geometric poloidal angle θ along the plasma boundary surface. As expected, at high pressure ($\beta_N = 2.78$), the fluid response significantly differs from the kinetic counterparts. The difference is however marginal at lower pressure ($\beta_N = 2.5$), i.e. well below the Troyon no-wall limit. The fundamental reason is that the marginal stability (and thus resonant field amplification) point, predicted by the fluid theory (i.e. the Troyon no-wall limit in our case), is not anymore a marginal point (and thus less amplification) when the kinetic stabilization is taken into account [28]. When the plasma is far from the marginal stability (e.g. at $\beta_N = 2.5$ in our case), no resonant field amplification occurs even according to the fluid theory [5]. Kinetic stabilization

in such a case thus plays a limited role in the plasma response, resulting in similar results as shown in Fig. 9(b).

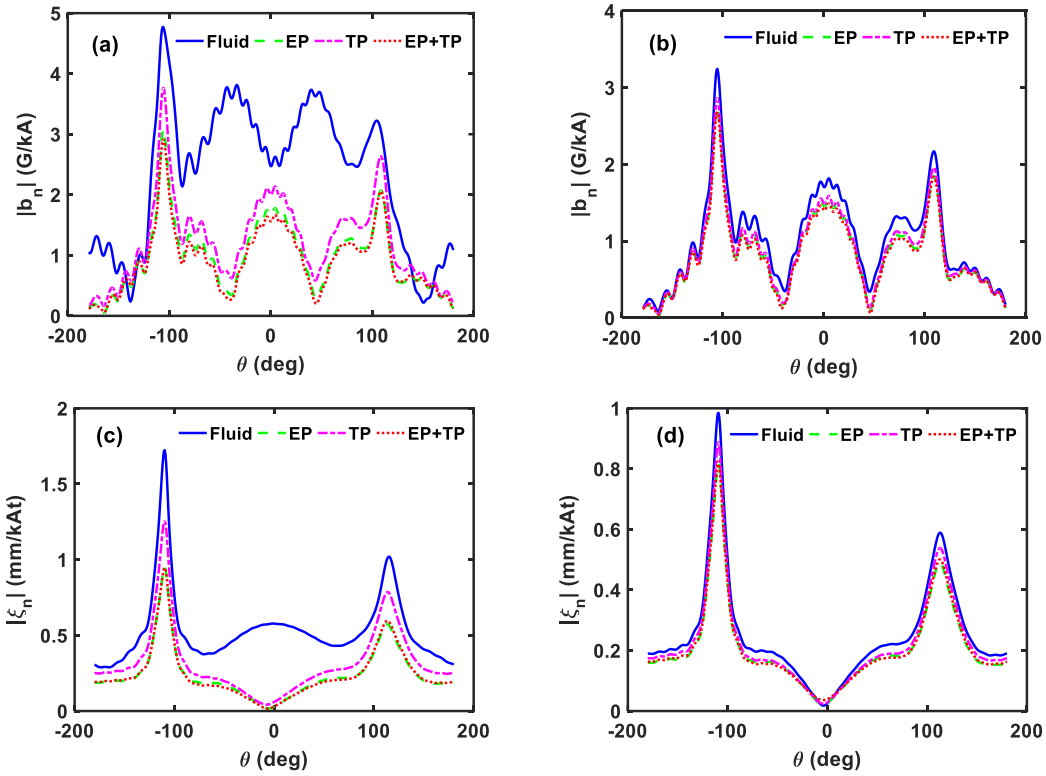

Figure 9. (Color online) Comparison of the amplitude of the normal component of the n=1 plasma response field along the plasma boundary surface (upper panels) and the plasma surface displacement (lower panels), for two equilibria with the normalized pressure at (a,c) $\beta_N = 2.78$ and (b,d) $\beta_N = 2.5$, respectively. Plotted is the fluid response computed by MARS-F ('Fluid'), together with various kinetic response due to the non-adiabatic contribution from energetic particles ('EP'), thermal particles ('TP') or both ('EP+TP'). θ is the geometrical poloidal angle along the plasma surface, with the origin defined at the magnetic axis, and with θ=0° corresponding to the outboard mid-plane of the torus. The on-axis rotation frequency is assumed to be $\Omega = 0.01\omega_A$. The RMP coils are located at $r_c = 1.9a$.

A better insight into the relative influence of each kinetic effect is obtained with Fig. 10, which compares the maximal amplitude and toroidal phase of the m/n=4/1 component of the radial field for the kinetic response, obtained by including a single kinetic effect once at a time in the MHD-kinetic hybrid computations. These single components include, for each particle species (thermal ions, thermal electrons, fusion born alphas), the precessional drift resonance of trapped particles, the bounce resonance of trapped particles, and the transit resonance of passing particles. For comparison, the dashed horizontal line indicates the fluid response and the dashed-dotted horizontal line indicates the full kinetic response including all resonance components and for all particle species. Therefore, the result that is close to the dashed horizontal line indicates a weak kinetic response, and the result that is close to the dash-dotted horizontal line indicates a strong kinetic effect.

Figure 10 shows that the precessional drift resonance of trapped thermal ions or trapped energetic particles plays the dominant a role in the kinetic response. Moreover, fusion-born alphas provide more kinetic contribution than thermal particles. Interestingly, the computed toroidal phase with inclusion of the non-adiabatic contribution (whichever type) from EPs alone agrees well with that predicted by the full kinetic effects. All these results indicate the importance of fusion born alphas in determining the kinetic response for the DEMO plasma considered here.

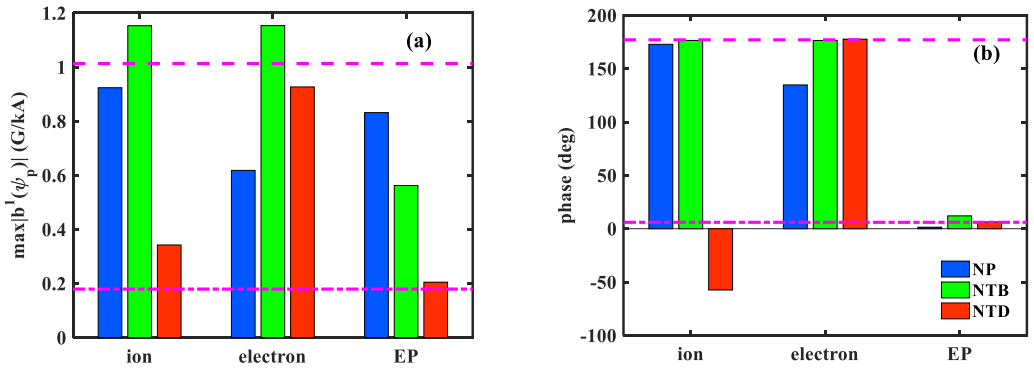

Figure 10. (Color online) The (a) maximal amplitude (along the plasma minor radius), and (b) associated toroidal phase, of the m=4/n=1 resonant radial magnetic field component, as a result of the plasma response to the applied n=1 RMP field in DEMO. Compared are the MHD-kinetic hybrid modeling results among three different groups assuming non-adiabatic drift kinetic contributions from a specific particle species (ions, electrons or fusion-born alphas ("EP")). Within each group, the field response due to the transit motion of passing particles ('NP'), the bounce motion of trapped particles ('NTB') and the precessional drift of trapped particles ('NTD') is also compared. The horizontal dashed and dash-dotted lines indicate the fluid response and the kinetic response including all particle contributions, respectively. Considered is the EU DEMO reference plasma with $\beta_N = 2.78$ and assuming the on-axis toroidal rotation of $\Omega = 0.01\omega_A$. The RMP coils are located at $r_c = 1.9a$.

3.4. Effect of parallel sound wave damping on n=1 plasma response

As mentioned earlier, a parallel sound wave damping (SWD) model is embedded in the MARS-F formulation, which acts as an effective viscous force on the parallel motion of the fluid. Physics-wise, this damping term describes Landau damping of the parallel sound waves due to the ion-acoustic resonances [45]. Previous modelling results (for other devices) indicate that a strong SWD better describes the experimental results in high β plasmas [27, 56], motivating our investigation presented in this subsection.

More specifically, we study sensitivity of the computed plasma (fluid) response with varying SWD damping coefficient $\kappa_{\|}$, ranging from no SWD ($\kappa_{\|} = 0$) to strong SWD ($\kappa_{\|} = 1.5$). The results are reported in Fig. 11, again in terms of the maximal amplitude and toroidal phase of the m/n=4/1 radial field perturbation. A sharp decay of the plasma response amplitude (Fig. 11(a)) is observed with initial increase of SWD up

to $\kappa_{\|} \le 0.5$, followed by a gradual saturation of the response with further increasing $\kappa_{\|}$. It is important to note that strong SWD damping (e.g. with $\kappa_{\|} = 1.5$) recovers well the response amplitude as predicted by the full kinetic response reported earlier, including both EPs and TPs. However, the toroidal phase of the response is not recovered, indicating that the SWD model still represents a crude fluid approximation of the full kinetic effects, as long as the plasma response in concerned.

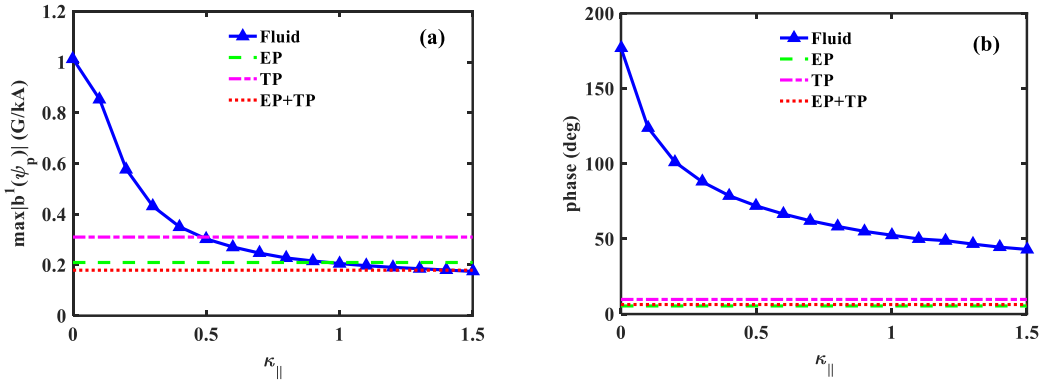

Figure 11. (Color online) The (a) maximal amplitude (along the plasma minor radius) and, (b) associated toroidal phase, of the *m*=4/*n*=1 resonant radial magnetic field component, as a result of the fluid response (solid line) to the applied *n*=1 RMP field in DEMO, while varying the parallel sound wave damping coefficient $\kappa_{\|}$. The horizontal lines indicate the kinetic response including the non-adiabatic drift kinetic contributions from fusion-born alphas ("EP", dashed line), thermal particle ('TP', dotted line) and both ('EP+TP', dash-dotted line), at $\kappa_{\|} = 0$. Considered is the EU DEMO reference plasma with $\beta_N = 2.78$ and assuming the on-axis toroidal rotation of $\Omega = 0.01\omega_A$. The RMP coils are located at $r_c = 1.9a$.

Damping of the plasma response due to strong SWD is also evident in the computed plasma distortion as shown in Fig 12, where amplitude of the *n*=1 radial displacement is compared between the no-SWD and strong-SWD ($\kappa_{\|} = 1.5$) cases. The plasma surface displacement, especially that near the outboard mid-plane, is markedly

reduced by the strong parallel sound wave damping. We also observe that the plasma surface displacement predicted by the strong SWD model nearly coincides with that by the full MHD-kinetic hybrid model (Fig. 12(a)), corroborating the result reported in Fig. 11(a). Furthermore, even the internal plasma displacement, as shown in the 2D plane in Fig. 12(b), resemble that obtained with the full kinetic effects (Fig. 8(d)). This results from the fact that the core kink response is also substantially damped by the strong SWD.

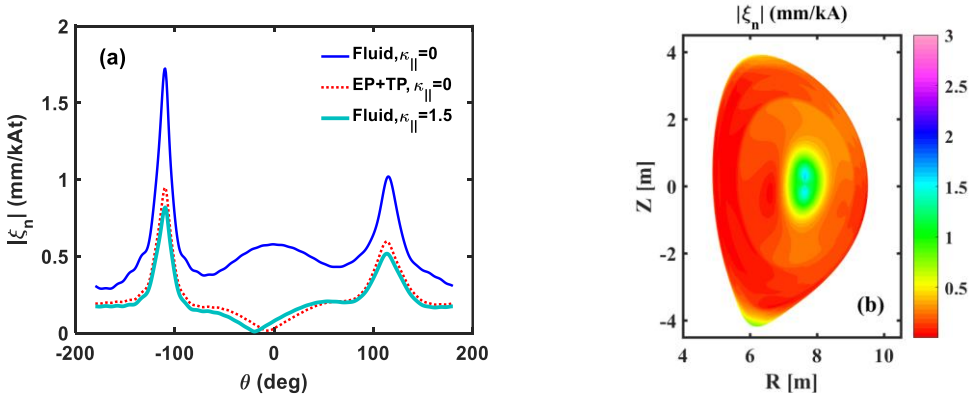

Figure 12. (Color online) (a) Comparison of the amplitude of the computed n = 1 plasma surface displacement versus the geometric poloidal angle among three models: the two fluid models with no-SWD (solid blue line) or with strong SWD ($\kappa_{||} = 1.5$, solid grey line), and the kinetic model with contributions from both fusion-born alphas and thermal particles ('EP+TP') but without SWD (dotted line). (b) The amplitude of the n = 1 radial plasma displacement in the poloidal 2D plane, assuming the latter model. Considered is the EU DEMO reference plasma with $\beta_N = 2.78$ and assuming the on-axis toroidal rotation of $\Omega = 0.01\omega_A$. The RMP coils are located at $r_c = 1.9a$.

3.5. Effect of radial location of RMP coils on plasma response

In what follows, we consider three radial locations of the mid-plane ELM control coils as illustrated in Fig. 1. Figure 13 compares the computed plasma response for the DEMO reference plasma, again in terms of the maximal amplitude and toroidal phase

of the *m*/*n*=4/1 resonant radial field component, assuming these three coil locations ($r_c = 1.9a$, $r_c = 2.6a$ and $r_c = 2.9a$). Compared are also three physics models for the plasma response – the fluid model with no-SWD ('F(0)') or strong SWD ('F(1.5)'), and the full kinetic model including contributions from thermal and energetic particles ('EP+TP').

First, we observe a larger plasma response with the RMP coils placed nearer the plasma, with the strongest response occurs for the in-vessel coils ($r_c = 1.9a$) among all three choices (Fig. 13(a)). This is as expected. Next, the plasma amplification is dramatically reduced by strong SWD or by full drift kinetic effects. In fact, both latter models generate nearly identical response field amplitude. Finally, we find that the toroidal phase of the computed response is insensitive to the radial location of the coils (Fig. 13(b)), though the phase is sensitive to the choice of the computational models as already illustrated by examples reported in earlier subsections. In particular, the full MHD-kinetic hybrid model predicts the smallest phase for the response field.

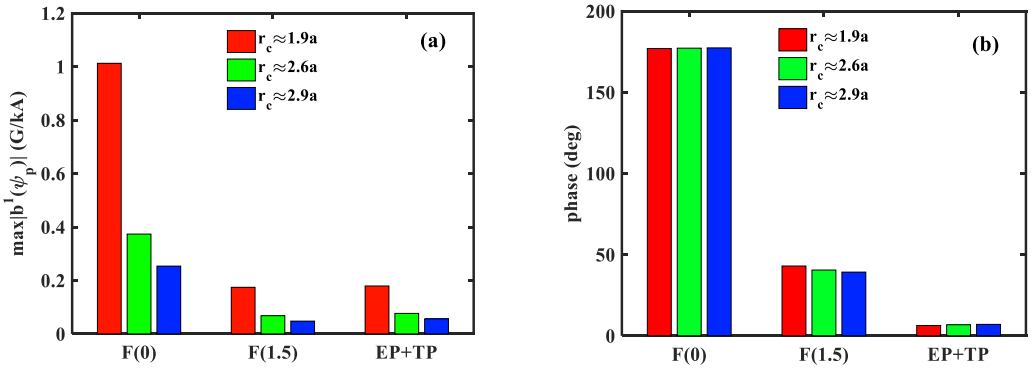

Figure 13. (Color online) The (a) maximal amplitude (along the plasma minor radius), and (b) associated toroidal phase, of the *m*=4/*n*=1 resonant radial magnetic field component, as a result of the plasma response to the applied *n*=1 RMP field in DEMO. Compared are the fluid response without or with a strong parallel sound wave damping, i.e., $\kappa_{\|} = 0$ ('F(0)') or $\kappa_{\|} = 1.5$ ('F(1.5)'), and the kinetic response including the non-adiabatic contribution from both fusion-born alphas and thermal particles ('EP+TP').

Within each group, comparison is also made among three radial locations of the RMP coils. Considered is the EU DEMO reference plasma with $\beta_N = 2.78$ and assuming the on-axis toroidal rotation of $\Omega = 0.01\omega_A$.

Similar comparison is also made for the modeled plasma surface displacement (Fig. 14), but for two choices of the coil location outside the DEMO vacuum vessel: $r_c \approx 2.6a$ and $r_c \approx 2.9a$. The displacement amplitude generally decays with the coil distance from the plasma, as expect. However, the relative variation of the displacement, with respect to the choice of three physics models, remains similar. In other words, irrespective of the coil location, the (pure) fluid model with no SWD results in considerably different plasma surface displacement, as compared to other two models which yield similar results. In particular, the pure fluid response has a large plasma displacement near the outboard mid-plane, which is often associated with the core-kink type of response [19, 40] as is also evident from Fig. 7.

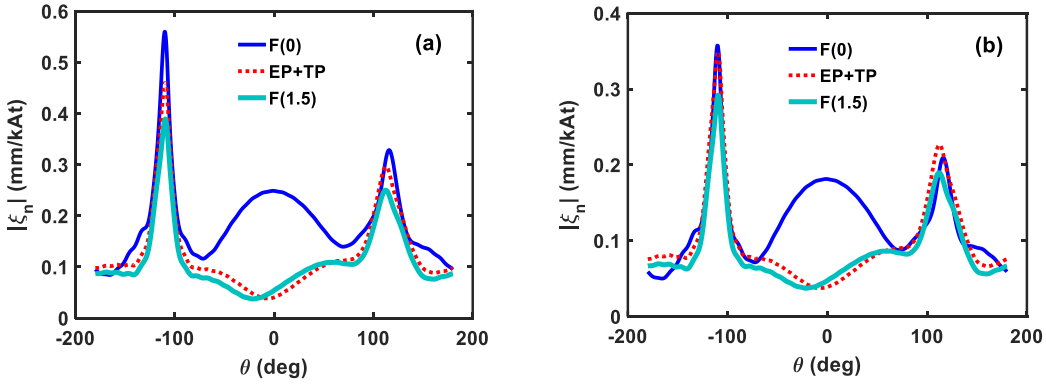

Figure 14. (Color online) Comparison of the amplitude of the computed n = 1 plasma surface displacement versus the geometric poloidal angle, between the fluid response without or with a strong parallel sound wave damping, i.e., $\kappa_{\|} = 0$ ('F(0)') or $\kappa_{\|} = 1.5$ ('F(1.5)'), and the kinetic response due to the non-adiabatic contribution from both fusion-born alphas and thermal particles ('EP+TP'), assuming two different radial locations of the ELM control coils at (a) $r_c \approx 2.6a$ or (b) $r_c \approx 2.9a$. Considered is

the EU DEMO reference plasma with $\beta_N = 2.78$ and assuming the on-axis toroidal rotation of $\Omega = 0.01\omega_A$.

3.6. Effect of the toroidal mode number n

We have so far been focusing on the plasma to the *n*=1 RMP field. As for the last part of study, we consider higher-*n* fields. With 16 independently powered coils along the toroidal angle according to the DEMO design, it is possible to design toroidal waveforms of the coil current to produce toroidal spectra up to *n*=8. Too high-*n* field however attenuates fast inside the plasma and therefore may not be the ideal choice. In what follows, we consider *n*=2-4. Note that 16-coil configuration is not the best for producing the *n*=3 field due to the periodicity constraint (large sideband may be expected). This is nevertheless not an issue with the MARS-F/K modeling, where we can assume a pure-*n* ELM control coil current as the source term.

We again scan the normalized plasma pressure while assuming different physics models for the plasma response, with the computed outermost resonant radial field component for each *n* reported in Fig. 15. Note that the outermost resonant field harmonic varies with *n*. For instance, the corresponding poloidal harmonic number is *m*=17 for the *n*=3 RMP, instead of *m*=4 for the *n*=1 case. Several important observations can be made here. First, unlike the *n*=1 response, the pure fluid response (with no SWD) is similar to the kinetic response for the DEMO target plasma and for the *n*=2 or 3 radial magnetic field. This hold for both the response field amplitude and phase, suggesting that the fluid approximation is adequate for modeling the plasma response to the *n*=2 or 3 RMP for the DEMO reference plasma. A fundamental reason is that the (computed) Troyon no-wall limit for the *n*=3 or 4 ideal kink instability well exceeds the designed target plasma pressure (Fig. 3(b-c)).

Next, we note the unusual non-monotonic behavior of the n=3 response field versus the equilibrium pressure, with a local peak near β_N~2.2 (Fig. 15(c)). This amplification effect is likely associated with a weakly unstable edge-peeling component, which has a local minimum near β_N=2 as shown in Fig. 3(c). The edge-peeling response is known to also produce resonant field amplification even before the plasma reaches the Troyon no-wall limit [17].

As for the final observation, we find a large amplification of the n=4 response for the target plasma (Fig. 15(e)), with either the fluid or kinetic models. Similar to the n=1 case, this amplification is due to proximity of the reference equilibrium pressure to the n=4 Troyon no-wall limit as reported in Fig 3(d). Indeed, for n=4, the DEMO target pressure of $\beta_N = 2.78$ is close to the inferred no-wall limit of $\beta_N^{NW} \sim 3.05$, i.e., $\beta_N / \beta_N^{NW} > 90\%$ (~91%), as compared with $\beta_N / \beta_N^{NW} \sim 83\%$ for the n=2 or 3 cases. On the other hand, a quantitative difference between the n=1 and n=4 response is that in the latter case, reduction of the response field amplitude (at the target pressure) by kinetic effects is not as drastic (only by a factor of about two) as that for the n=1 case. The main reason is that with the n=4 RMP, the field amplification is associated with higher number resonant poloidal harmonics (shown is m=17 or 18 in Fig. 15(e)) which is largely localized near the plasma edge. Drift kinetic damping due to bulk thermal particles, as well as from fusion-born alphas, is therefore less efficient.

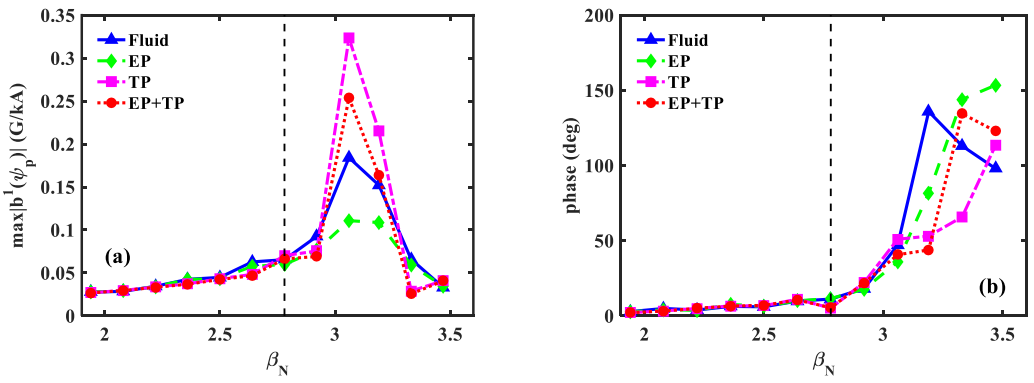

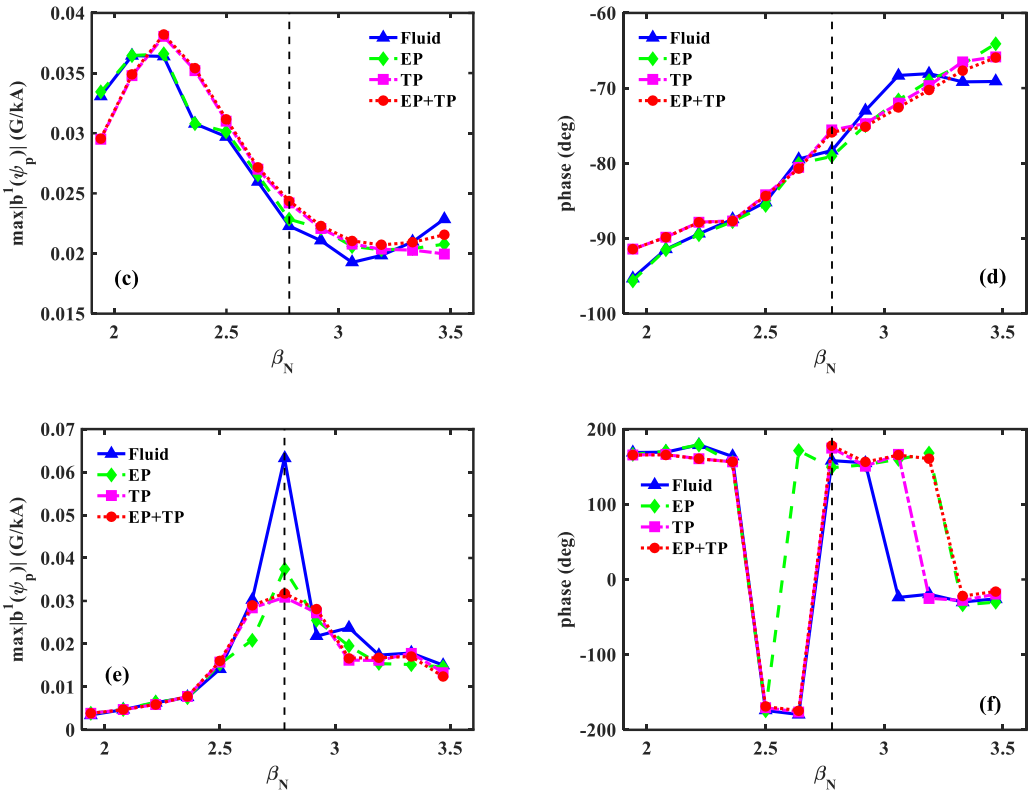

Figure 15. (Color online) The (a) maximal amplitude (along the minor radius), and (b) associated toroidal phase, of the radial magnetic field b^1 for the outermost resonant poloidal Fourier harmonic m inside the plasma, with (a,b) n=2, m=8 or 9, (c,d) n=3, m=17 and (e,f) n=4, m=17 or 18, plotted versus the normalized plasma pressure β_N and assuming the (on-axis) toroidal rotation frequency of $\Omega = 0.01\omega_A$. Compared are the response fields computed assuming the fluid model ('Fluid'), and the MHD-kinetic hybrid model including the non-adiabatic contributions from fusion-born alphas ("EP"), thermal particles ('TP'), or both ('EP+TP'). Vertical dashed lines indicate the DEMO design value of $\beta_N = 2.78$. The RMP coils are located at $r_c = 1.9a$.

4. Summary

We have carried out a systematic investigation on the plasma response to the externally applied RMP field for the purpose of controlling ELMs in an EU DEMO reference

plasma. A particular emphasis is on the role of kinetic effects, from both thermal particles and fusion-born alphas, in the modeled plasma response. This is motivated by the fact that the target equilibrium pressure is close to the computed Troyon no-wall limits, especially for the n=1 perturbation. As for the modeling tools, we employ both the MARS-F and MARS-K codes, both taking into account the full toroidal geometry, the effects of the finite plasma resistivity and the plasma equilibrium toroidal rotation.

Similar to previous studies carried out for the DIII-D [28] and NSTX [32] experiments, we find that the n=1 plasma response amplitude grows nearly linearly with the normalized equilibrium pressure, when the latter is well below the Troyon no-wall limit ($\beta_N < 2.5$ in our case). In this range, the kinetic effects, as well as the plasma toroidal rotation, play a minor role in determining the plasma response. However, when the plasma pressure reaches the target value of $\beta_N = 2.78$ according to the DEMO design, the fluid model predicts a large peak amplification. This amplification mainly occurs for the poloidal harmonics with positive helicity (i.e. m>0) in the whole spectral domain. Strongest amplification occurs for the non-resonant portion of the spectrum (m=2) in the plasma core for this EU DEMO design, due to the presence of a marginally stable kink mode.

On the other hand, a more advanced plasma response model, including kinetic resonances between the RMP perturbation and drift motions of thermal and energetic particles, finds strong suppression of the n=1 field amplification for the DEMO reference plasma as compared to the pure fluid prediction. In particular, we find that the kinetic effect from fusion-born α-particles, especially that associated with the precessional drift resonance, plays a major role in reducing the response amplitude near the Troyon no-wall limit. This is different from the present-day devices (DIII-D and NSTX), where the kinetic effects for damping the plasma response mainly come from thermal particles. These findings have direct implications for ELM control in DEMO

with the RMP field, since a pure single-fluid model would produce a too optimistic prediction for the coil current requirement according to semi-empirical criteria established based on present-day ELM control experiments [19, 33, 40].

Interestingly, we also find that a strong parallel sound wave damping model (with $\kappa_{\|} = 1.5$), implemented into the MARS-F fluid response model, well reproduces the full kinetic response results for the DEMO target plasma, in terms of both the resonant field response amplitude and the plasma displacement. The toroidal phase of the response field, however, does not match between the strong SWD model and the full drift kinetic model, indicating the deficit of the former in predicting the plasma response. These results hold independent of the radial location of the ELM control coils that we assume for DEMO.

Finally, both fluid and kinetic models produce similar response for the *n*=2 and 3 RMP fields for the considered DEMO plasma, mainly because the target equilibrium is well below the predicted no-wall limit for the corresponding toroidal spectrum. The kinetic effect again becomes important for the *n*=4 RMP, due to proximity of the reference plasma to the no-wall limit for the *n*=4 ideal kink instability. The effect is however less drastic as compared to the *n*=1 RMP, because drift kinetic resonances from bulk thermal particles and fusion-born alphas are less effective in damping high-*m* perturbations (with *n*=4) that are more localized near the plasma edge.

As a final remark, we emphasize that this work only focuses on computing the plasma response to the RMP field for DEMO, in particular considering the role of drift kinetic resonances. No explicit results on the coil current requirement for ELM control in DEMO are produced. A first-principle prediction of the coil current requires non-linear full MHD simulations (or even beyond given the importance of the kinetic effects as found in this work), which is beyond the scope of the present study. Note also that other types of energetic particles (e.g. those due to neutral beam injection), than the

fusion-born alphas, are not included in this study. These EPs may also affect the plasma response (though their effect on RFA was found to be insignificant in DIII-D [28]), and will be considered in future studies as accurate models for these particles will be available for EU DEMO.

Acknowledgments

This work is supported by 'the Fundamental Research Funds for the Central Universities' (Grant Numbers 3132020181, 3132021200, 3132022195), and by National Natural Science Foundation of China (NSFC) (Grant Nos. 11975062 and 11905022). The work is also supported by the U.S. DoE Office of Science under Contract Nos. DE-FG02-95ER54309 and DE-FC02-04ER54698.

References

[1] Loarte A *et al* 2007 Nucl. Fusion **47** S203-S263
[2] Siccinio M *et al* 2020 Fusion Eng. Design **156** 111603
[3] Evans T E *et al* 2004 Phys. Rev. Lett. **92** 235003
[4] Lanctot M J *et al* 2010 Phys. Plasmas **17** 030701
[5] Liang Y *et al* 2007 Phys. Rev. Lett. **98** 265004
[6] Park J-K, Boozer A H, Menard J E, Gerhardt S P, Sabbagh S A 2009 Phys. Plasmas **16** 082512
[7] Kirk A *et al* 2010 Nucl. Fusion **50** 034008
[8] Kirk A *et al* 2015 Nucl. Fusion **55** 043011
[9] Suttrop W *et al* 2011 Phys. Rev. Lett. **106** 225004
[10] Jeon Y M *et al* 2012 Phys. Rev. Lett. **109** 035004
[11] Sun Y *et al* 2016 Phys. Rev. Lett. **117** 115001
[12] Liu Y *et al* 2017 Phys. Plasmas **24** 056111
[13] Bécoulet M *et al* 2008 Nucl. Fusion **48** 024003
[14] Heyn M F, Ivanov I B, Kasilov S V, Kernbichler W, Joseph I, Moyer R A, Runov A M 2008 Nucl. Fusion **48** 024005
[15] Liu Y, Kirk A, Nardon E 2010 Phys. Plasmas **17** 122502
[16] Park G, Chang C S, Joseph I, Moyer R A 2010 Phys. Plasmas **17** 102503
[17] Liu Y, Saarelma S, Gryaznevich M P, Hender T C, Howell D F 2010 Plasma Phys. Control. Fusion **52** 045011
[18] Lanctot M J *et al* 2011 Phys. Plasmas **18** 056121
[19] Liu Y, Kirk A, Gribov Y, Gryaznevich M P, Hender T C, Nardon E 2011 Nucl. Fusion **51** 083002

[20] Chapman I T, Cooper W A, Kirk A, Ham C J, Harrison J R, Patel A, Pinches S D, Scannell R, Thornton A J 2012 Plasma Phys. Control. Fusion **54** 105013
[21] Ferraro N M 2012 Phys. Plasmas **19** 056105
[22] Liu Y Q, Kirk A, Sun Y, Cahyna P, Chapman I T, Denner P, Fishpool G, Garofalo A M, Harrison J R, Nardon E 2012 Plasma Phys. Control. Fusion **54** 124013
[23] Evans T E, Orlov D M, Wingen A, Wu W, Loarte A, Casper T A, Schmitz O, Saibene G, Schaffer M J, Daly E 2013 Nucl. Fusion **53** 093029
[24] Evans T E 2013 Journal of Nuclear Materials **438** S11-S18
[25] Haskey S R, Lanctot M J, Liu Y Q, Hanson J M, Blackwell B D, Nazikian R 2014 Plasma Phys. Control. Fusion **56** 035005
[26] Liu Y *et al* 2015 Nucl. Fusion **55** 063027
[27] Liu Y *et al* 2016 Nucl. Fusion **56** 056015
[28] Wang Z R, Lanctot M J, Liu Y Q, Park J K, Menard J E 2015 Phys. Rev. Lett. **114** 145005
[29] Yang X, Sun Y, Liu Y, Gu S, Liu Y, Wang H, Zhou L, Guo W 2016 Plasma Phys. Control. Fusion **58** 114006
[30] Zhou L, Liu Y, Liu Y, Yang X 2016 Plasma Phys. Control. Fusion **58** 115003
[31] Li L, Liu Y Q, Wang N, Kirk A, Koslowski H R, Liang Y, Loarte A, Ryan D, Zhong F C 2017 Plasma Phys. Control. Fusion **59** 044005
[32] Wang Z, Park J-K, Menard J E, Liu Y, Kaye S M, Gerhardt S 2018 Nucl. Fusion **58** 016015
[33] Zhou L, Liu Y, Wenninger R, Liu Y, Wang S, Yang X 2018 Nucl. Fusion **58** 076025
[34] Gu S *et al* 2019 Nucl. Fusion **59** 026012
[35] Weisberg D B, Paz-Soldan C, Liu Y Q, Logan N C 2019 Nucl. Fusion **59** 086060
[36] Hu Q M, Nazikian R, Grierson B A, Logan N C, Orlov D M, Paz-Soldan C, Yu Q 2020 Phys Rev Lett **125** 045001
[37] Liu Y, Lyons B C, Gu S, Kirk A, Li L, Paz-Soldan C, Shafer M W, Turnbull A D 2021 Plasma Phys. Control. Fusion **63** 065003
[38] Hao G Z *et al* 2021 Nucl. Fusion **61** 126031
[39] Yang X, Liu Y, Xu W, He Y, Lu S 2021 Nucl. Fusion **62** 016013
[40] Liu Y, Ham C J, Kirk A, Li L, Loarte A, Ryan D A, Sun Y, Suttrop W, Yang X, Zhou L 2016 Plasma Phys. Control. Fusion **58** 114005
[41] Rozhansky V, Kaveeva E, Molchanov P, Veselova I, Voskoboynikov S, Coster D, Kirk A, Lisgo S, Nardon E 2010 Nucl. Fusion **50** 034005
[42] Liu Y, Connor J W, Cowley S C, Ham C J, Hastie R J, Hender T C 2012 Phys. Plasmas **19** 072509
[43] Liu Y, Chu M S, Chapman I T, Hender T C 2008 Phys. Plasmas **15** 112503
[44] Liu Y, Kirk A, Keeling D L, Kogan L, Du X D, Li L, Piron L, Ryan D A, Turnbull A D 2021 Nucl. Fusion **61** 116022
[45] Hammett G W, Perkins F W 1990 Phys. Rev. Lett. **64** 3019-3022
[46] Bondeson A, Iacono R 1989 Physics of Fluids B: Plasma Physics **1** 1431-1443
[47] Liu Y, Chapman I T, Saarelma S, Gryaznevich M P, Hender T C, Howell D F 2009 Plasma Phys. Control. Fusion **51** 115005
[48] Hu B, Betti R, Manickam J 2006 Phys. Plasmas **13** 112505
[49] Federici G *et al* 2019 Nucl. Fusion **59** 066013
[50] Fable E *et al* 2013 Plasma Phys. Control. Fusion **55** 124028

[51] Hirvijoki E, Asunta O, Koskela T, Kurki-Suonio T, Miettunen J, Sipilä S, Snicker A, Äkäslompolo S 2014 Computer Physics Communications **185** 1310-1321
[52] Liu Y 2010 Nucl. Fusion **50** 095008
[53] Gaffey J D, Jr., 1976 J. Plasma Physics **16** 149-169
[54] Troyon F, Gruber R, Saurenmann H, Semenzato S, Succi S 1984 Plasma Phys. Control. Fusion **26** 209
[55] Wang Z R *et al* 2019 Nucl. Fusion **59** 024001
[56] Liu Y *et al* 2005 Nucl. Fusion **45** 1131